LA-7722-PR
Progress Report

C.3

Applied Nuclear Data Research and Development

October 1—December 31, 1978

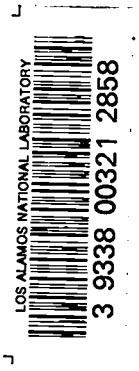

LOS ALAMOS SCIENTIFIC LABORATORY
Post Office Box 1663 Los Alamos, New Mexico 87545

The four most recent reports in this series, unclassified, are LA-7200-PR, LA-7301-PR, LA-7482-PR, and LA-7596-PR.

This work was performed under the auspices of the Electric Power Research Institute and the US Department of Energy's Office of Military Application, Division of Reactor Research and Technology, Office of Basic Energy Sciences, and Office of Fusion Energy.

UNITED STATES
DEPARTMENT OF ENERGY
CONTRACT W-7405-ENG. 36

LA-7722-PR
Progress Report
Special Distribution
Issued: March 1979

Applied Nuclear Data Research and Development

October 1—December 31, 1978

Compiled by
C. I. Baxman
P. G. Young

CONTENTS

I. THEORY AND EVALUATION OF NUCLEAR CROSS SECTIONS..... 1
A. Fusion Reactions..... 1
B. Calculation of Cross Sections for Yttrium and Zirconium.. 2
C. Fission Spectrum Workshop..... 11
D. Calculation of Prompt Fission Neutron Spectra..... 11
E. LASL Version of NMTC..... 13
F. Summary Documentation of LASL Evaluations for ENDF/B-V... 15
II. NUCLEAR CROSS-SECTION PROCESSING..... 15
A. Space-Energy Collapse..... 15
B. Discrete Angle Representation of Thermal Neutron Scattering..... 16
C. Testing Data and Methods Effects on JEZEBEL and GODIVA... 18
D. Gamma-Ray Spectra of Activation Products..... 19
III. FISSION PRODUCTS AND ACTINIDES: YIELDS, YIELD THEORY, DECAY DATA, DEPLETION, AND BUILDUP..... 21
A. Fission Yield Theory..... 21
B. ENDF/B-V Yields..... 22
C. ENDF/B-V Average Energies..... 22
D. CINDER-10/ORIGEN Comparison..... 23
E. Fission Product Gamma Spectra..... 23
F. The Effects of Neutron Absorption on Decay Heat..... 24
REFERENCES..... 27

APPLIED NUCLEAR DATA RESEARCH AND DEVELOPMENT
QUARTERLY PROGRESS REPORT
October 1 - December 31, 1978

Compiled by

C. I. Baxman and P. G. Young

ABSTRACT

This progress report describes the activities of the Los Alamos Nuclear Data Group for the period October 1 through December 31, 1978. The topical content is summarized in the contents.

I. THEORY AND EVALUATION OF NUCLEAR CROSS SECTIONS

A. Fusion Reactions (G. Hale)

Many of our R-matrix studies in light nuclei have been directed at obtaining reliable cross sections and Maxwellian-averaged reaction rates for the primary fusion reactions as well as for secondary reactions that can occur in some designs. During the past quarter, we have continued to study the t + T reactions, and have calculated reaction rates for the p + ^{6}Li and p + T reactions.

Adding the measurements of Agnew et al.[1] to our analysis of reactions in the ^{6}He system resulted in essentially the same low-energy T(t,2n)^{4}He cross sections as were obtained before[2] but raised the cross sections $\sim$30% at energies near 2 MeV. The changes in the predicted cross sections around 2 MeV had little effect on the reaction rates for temperatures below kT = 100 keV, however.

The new fit to T(t,2n) cross-section measurements is shown in Fig. 1. The bump evident in the calculations and in the experimental data[1] at around 2 MeV appears to correspond with a broad level observed in ^{6}He at about 13.6 MeV excitation energy. The data in the analysis, which include T(t,t)T angular distributions between 1.6 and 2 MeV,[3] are not inconsistent with an assignment of $J^{\pi} = 0^{+}$ for this level, although other possibilities have not yet been tried.

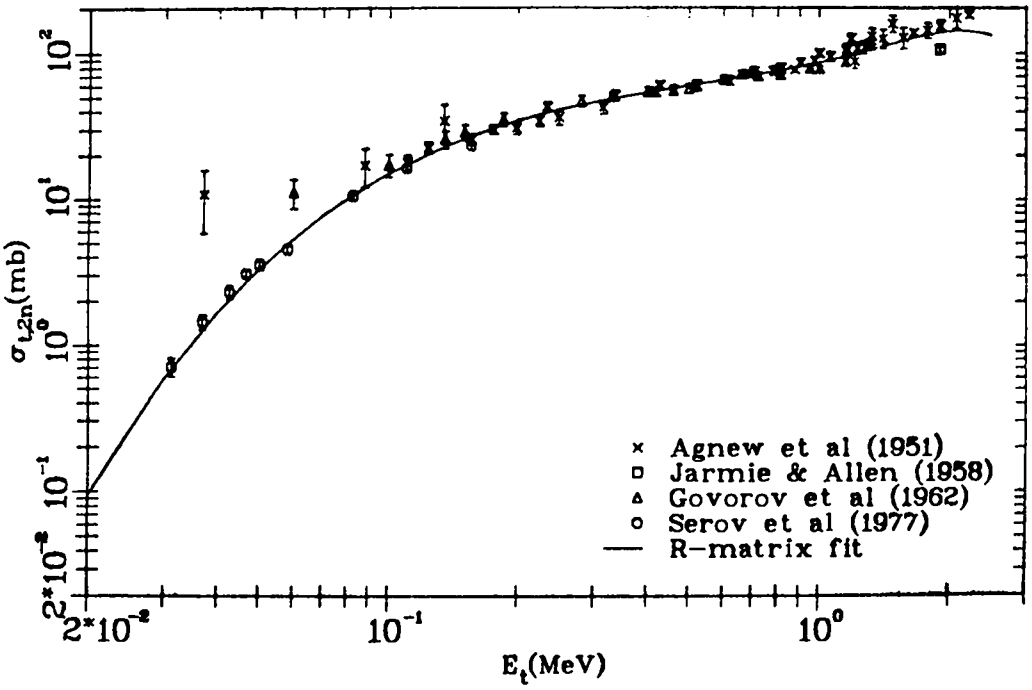

Fig. 1.
R-matrix fit (solid curve) compared to measurements for the T(t,2n) ^{4}He cross section at energies between 0.2 and 2.5 MeV.

Maxwellian-averaged reaction rates for ^{6}Li(p,^{3}He)^{4}He and T(p,n)^{3}He have been calculated using cross sections from our R-matrix studies of reactions in the 7- and 4-nucleon systems. The p + ^{6}Li reaction rate rises monotonically from 10^{-25} cm^3/s at kT = 1 keV to 2 x 10^{-16} cm^3/s at kT = 1 MeV. The 1 MeV threshold for the p + T reaction makes its reaction rate negligible for kT below 10 keV, but it rises rapidly to overtake the p + ^{6}Li reaction rate at kT = 300 keV.

B. Calculation of Cross Sections for Yttrium and Zirconium (E. D. Arthur)

Calculations using the GNASH and COMNUC nuclear-model codes have been made for 104 neutron-induced reaction cross sections on isotopes of yttrium and zirconium. Table I lists the reactions for which calculations were made between threshold and 20 MeV. For those reactions having positive Q values, the calculations have been supplemented with cross-section estimates down to energies of 10^{-5} eV.

An extensive effort towards the determination of input parameters was made for this series of calculations. A modified form of the Lagrange parameter set[4]

TABLE I

Q-VALUES AND THRESHOLDS FOR YTTRIUM AND ZIRCONIUM REACTIONS

MAT	MT	Reaction	Final State[a]	Q (MeV)	E_{th} (MeV)
3986	4	$^{86}Y(n,n')^{86}Y$	0	- 0.208	0.210
	16	$^{86}Y(n,2n)^{85}Y$	0	- 9.473	9.584
	16	$^{86}Y(n,2n)^{85m}Y$	1	- 9.493	9.604
	22	$^{86}Y(n,n\alpha)^{82}Rb$	0	- 5.43	5.494
	28	$^{86}Y(n,np + n,pn)^{85}Sr$	0	- 5.669	5.736
	52	$^{86}Y(n,n')^{86m}Y$	2	- 0.218	0.221
	102	$^{86}Y(n,\gamma)^{87}Y$	0	11.82	--
	103	$^{86}Y(n,p)^{86}Sr$	0	6.055	--
	107	$^{86}Y(n,\alpha + n,\alpha n)^{83,82}Rb$	0	5.359	--
3987	4	$^{87}Y(n,n')^{87}Y$	0	- 3.81	0.386
	16	$^{87}Y(n,2n)^{86}Y$	0	-11.82	11.96
	16	$^{87}Y(n,2n)^{86m}Y$	2	-12.04	12.17
	22	$^{87}Y(n,n\alpha)^{83}Rb$	0	- 6.46	6.535
	28	$^{87}Y(n,np + n,pn)^{86}Sr$	0	- 5.764	5.831
	51	$^{87}Y(n,n')^{87m}Y$	1	- 3.81	0.386
	102	$^{87}Y(n,\gamma)^{88}Y$	0	9.377	--
	103	$^{87}Y(n,p)^{87}Sr$	0	2.665	--
	103	$^{87}Y(n,p)^{87m}Sr$	1	2.276	--
	107	$^{87}Y(n,\alpha + n,\alpha n)^{84,83}Rb$	0	2.416	--
3988	4	$^{88}Y(n,n')^{88}Y$	0	- 0.232	0.235
	16	$^{88}Y(n,2n)^{87}Y$	0	- 9.376	9.484
	16	$^{88}Y(n,2n)^{87m}Y$	1	- 9.758	9.87
	22	$^{88}Y(n,n\alpha)^{84}Rb$	0	- 3.73	3.773
	28	$^{88}Y(n,np + n,pn)^{87}Sr$	0	- 6.712	6.789
	28	$^{88}Y(n,np + n,pn)^{87m}Sr$	1	- 7.1	7.182
	52	$^{88}Y(n,n')^{88m1}Y$	2	- 0.393	0.398
	53	$^{88}Y(n,n')^{88m2}Y$	3	- 0.675	0.683
	102	$^{88}Y(n,\gamma)^{89}Y$	0	11.468	--
	103	$^{88}Y(n,p)^{88}Sr$	0	4.401	--
	107	$^{88}Y(n,\alpha + n,\alpha n)^{85,84}Rb$	0	3.517	--

TABLE I (cont)

MAT	MT	Reaction	Final State[a]	Q (MeV)	E_{th} (MeV)
3989	4	$^{89}Y(n,n')^{89}Y$	0	- 0.908	0.918
	16	$^{89}Y(n,2n)^{88}Y$	0	-11.468	11.598
	16	$^{89}Y(n,2n)^{88m1}Y$	2	-11.86	11.96
	16	$^{89}Y(n,2n)^{88m2}Y$	3	-12.143	12.281
	22	$^{89}Y(n,n\alpha)^{85}Rb$	0	- 7.95	8.04
	28	$^{89}Y(n,np + n,pn)^{88}Sr$	0	- 7.07	7.147
	51	$^{89}Y(n,n')^{89m}Y$	1	- 9.08	0.918
	102	$^{89}Y(n,\gamma)^{90}Y$	0	6.86	--
	102	$^{89}Y(n,\gamma)^{90m}Y$	2	6.178	--
	103	$^{89}Y(n,p)^{89}Sr$	0	- 0.707	0.715
	107	$^{89}Y(n,\alpha + n,\alpha n)$	0	0.699	--
3990	4	$^{90}Y(n,n')^{90}Y$	0	- 0.203	0.205
	16	$^{90}Y(n,2n)^{89}Y$	0	- 6.86	6.937
	16	$^{90}Y(n,2n)^{89m}Y$	1	- 7.768	7.855
	17	$^{90}Y(n,3n)^{88}Y$	0	-18.33	18.53
	22	$^{90}Y(n,n\alpha)^{86}Rb$	0	- 6.16	6.23
	28	$^{90}Y(n,np + n,pn)^{89}Sr$	0	7.567	7.652
	52	$^{90}Y(n,n')^{90m}Y$	2	- 0.685	0.693
	102	$^{90}Y(n,\gamma)^{91}Y$	0	7.946	--
	103	$^{90}Y(n,p)^{90}Sr$	0	0.237	--
	107	$^{90}Y(n,\alpha + n,\alpha n)^{87,86}Rb$	0	3.765	--
3991	4	$^{91}Y(n,n')^{91}Y$	0	- 0.556	0.562
	16	$^{91}Y(n,2n)^{90}Y$	0	- 7.946	8.034
	16	$^{91}Y(n,2n)^{90m}Y$	2	- 8.63	8.727
	17	$^{91}Y(n,3n)^{89}Y$	0	-14.81	14.97
	17	$^{91}Y(n,3n)^{89m}Y$	1	-15.71	15.89
	22	$^{91}Y(n,n\alpha)^{87}Rb$	0	- 4.18	4.23
	28	$^{91}Y(n,np + n,pn)^{90}Sr$	0	- 7.709	7.759
	51	$^{91}Y(n,n')^{91m}Y$	1	- 0.556	0.562
	102	$^{91}Y(n,\gamma)^{92}Y$	0	6.557	--
	103	$^{91}Y(n,p)^{91}Sr$	0	- 1.883	1.903
	107	$^{91}Y(n,\alpha + n,\alpha n)^{88,87}Rb$	0	1.902	--

TABLE I (Cont)

MAT	MT	Reaction	Final State[a]	Q (MeV)	E_{th} (MeV)
3992	4	$^{92}Y(n,n')^{92}Y$	0	- 0.28	0.283
	16	$^{92}Y(n,2n)^{91}Y$	0	- 6.557	6.629
	16	$^{92}Y(n,2n)^{91m}Y$	1	- 7.113	7.191
	17	$^{92}Y(n,3n)^{90}Y$	0	-14.5	14.66
	17	$^{92}Y(n,3n)^{90m}Y$	2	-15.19	15.35
	22	$^{92}Y(n,n\alpha)^{88}Rb$	0	- 4.655	4.706
	28	$^{92}Y(n,np + n,pn)^{91}Sr$	0	- 8.44	8.532
	102	$^{92}Y(n,\gamma)^{93}Y$	0	7.49	--
	103	$^{92}Y(n,p)^{92}Sr$	0	- 1.13	1.14
	107	$^{92}Y(n,\alpha + n,\alpha n)^{89,88}Rb$	0	2.52	--
4088	4	$^{88}Zr(n,n')^{88}Zr$	0	- 1.058	1.07
	16	$^{88}Zr(n,2n)^{87}Zr$	0	-12.2	12.34
	16	$^{88}Zr(n,2n)^{87m}Zr$	2	-12.536	12.68
	22	$^{88}Zr(n,n\alpha)^{84}Sr$	0	- 5.397	5.449
	28	$^{88}Zr(n,np + n,pn)^{87}Y$	0	- 7.917	8.01
	28	$^{88}Zr(n,np + n,pn)^{87m}Y$	1	- 8.298	8.39
	102	$^{88}Zr(n,\gamma)^{89}Zr$	0	9.312	--
	103	$^{88}Zr(n,p)^{88}Y$	0	1.462	--
	103	$^{88}Zr(n,p)^{88m1}Y$	2	1.069	--
	103	$^{88}Zr(n,p)^{88m2}Y$	3	0.787	-
	107	$^{88}Zr(n,\alpha + n,\alpha n)^{85,84}Sr$	0	3.13	--
4089	4	$^{89}Zr(n,n')^{89}Zr$	0	- 0.587	0.594
	16	$^{89}Zr(n,2n)^{88}Zr$	0	- 9.311	9.417
	22	$^{89}Zr(n,n\alpha)^{85}Sr$	0	- 6.18	6.25
	28	$^{89}Zr(n,np + n,pn)^{88}Y$	0	- 7.853	7.941
	28	$^{89}Zr(n,np + n,pn)^{88m1}Y$	2	- 8.245	8.339
	28	$^{89}Zr(n,np + n,pn)^{88m2}Y$	3	- 8.527	8.624
	51	$^{89}Zr(n,n')^{89m}Zr$	1	- 0.587	0.594
	102	$^{89}Zr(n,\gamma)^{90}Zr$	0	11.983	--
	103	$^{89}Zr(n,p)^{89}Y$	0	3.616	--
	103	$^{89}Zr(n,p)^{89m}Y$	1	2.708	--
	107	$^{89}Zr(n,\alpha + n,\alpha n)^{86,85}Sr$	0	5.305	--

TABLE I (cont)

MAT	MT	Reaction	Final State[a]	Q (MeV)	E_{th} (MeV)
4090	4	$^{90}Zr(n,n')^{90}Zr$	0	- 1.76	1.78
	16	$^{90}Zr(n,2n)^{89}Zr$	0	-11.983	12.117
	16	$^{90}Zr(n,2n)^{89m}Zr$	1	-12.57	12.71
	22	$^{90}Zr(n,n\alpha)^{86}Sr$	0	- 6.678	6.753
	28	$^{90}Zr(n,np + n,pn)^{89}Y$	0	- 8.366	8.46
	28	$^{90}Zr(n,np + n,pn)^{89m}Y$	1	- 9.27	9.38
	102	$^{90}Zr(n,\gamma)^{91}Zr$	0	7.203	--
	103	$^{90}Zr(n,p)^{90}Y$	0	- 1.506	1.523
	103	$^{90}Zr(n,p)^{90m}Y$	2	- 2.19	2.216
	107	$^{90}Zr(n,\alpha + n,\alpha n)^{87,88}Sr$	0	1.75	--

[a] The convention used here is that for a particular reaction a final state of 0 signifies that the cross section listed is the total cross section for that reaction, not just the amount leading to the ground state. If the final state is not equal to 0, then the cross section listed is that for population of the indicated isomeric state.

for ^{89}Y, applicable over the energy range from 0.010 to 20 MeV, was used to generate neutron-transmission coefficients. Proton parameters were based on a recent set of Johnson et al.[5] utilizing sub-Coulomb barrier (p,n) data.

Finally, reaction channels involving gamma-ray emission were determined from fits[6] to neutron capture cross sections for A=80-99. As in our previous calculations,[7] we used the Gilbert-Cameron level density expressions[8] with Cook parameters.[9] A new and more complete preequilibrium formalism based on the exciton model of Kalbach[10] was used to provide a more realistic description of non-statistical effects.

These calculations utilized information resulting from new cross-section data on unstable yttrium and zirconium isotopes. Also, charged-particle production cross sections measured through simulation of neutron-induced reactions were important in these parameter determinations.[11]

In Figs. 2-9, the general trends of selected cross sections are displayed as a function of isotope and neutron energy. These figures will comprise part of an upcoming Los Alamos Scientific Laboratory report describing these calculations in detail.

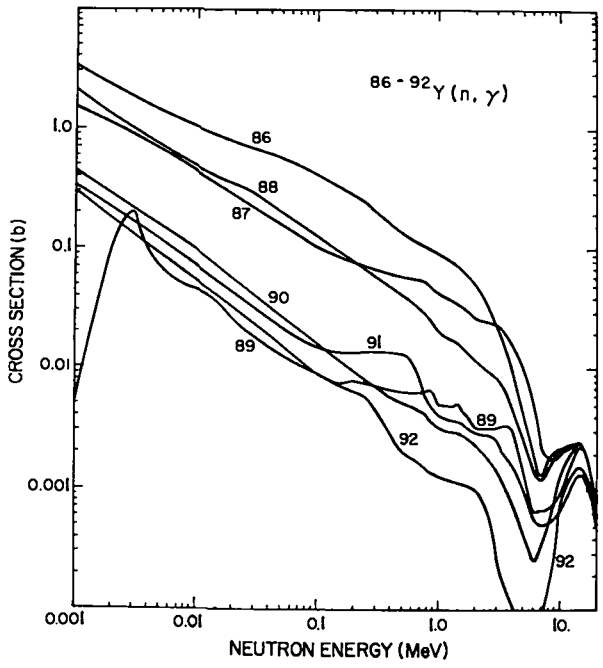

Fig. 2.
Calculated capture cross section for yttrium isotopes. For ^{89}Y below 0.007 MeV, the curve was drawn to include resonance effects indicated by experimental data.

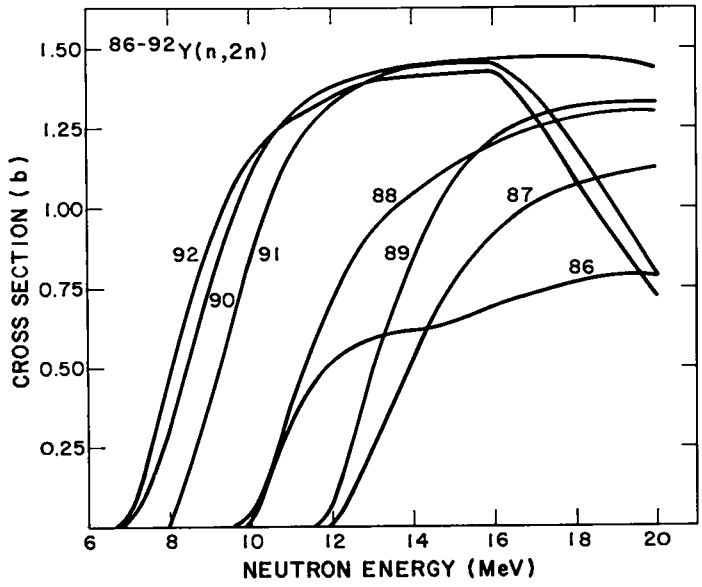

Fig. 3.
Calculated $^{86-92}Y(n,2n)$ cross sections. Above 16 MeV, the $^{91,92}Y(n,2n)$ cross sections decrease because of (n,3n) competitions. For $^{86,87}Y$, significant charged-particle emission lowers the cross section.

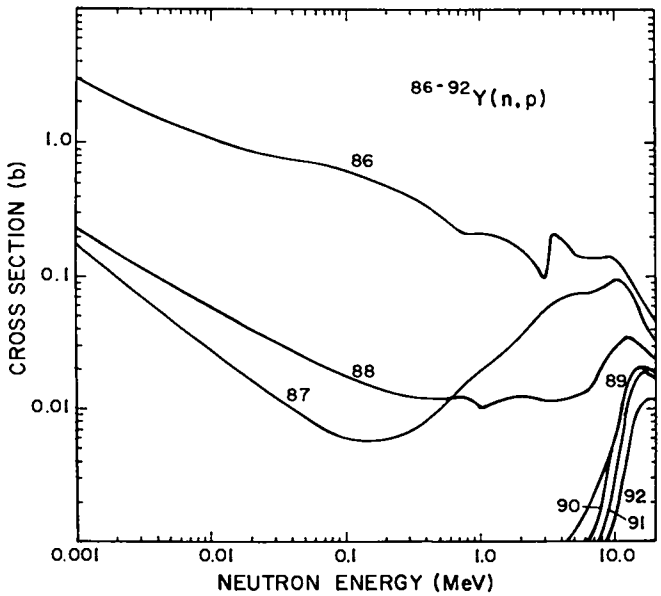

Fig. 4.
Calculated (n,p) cross sections. The $^{86-88}$Y(n,p) reactions have large positive Q values leading to appreciable cross sections at low energies.

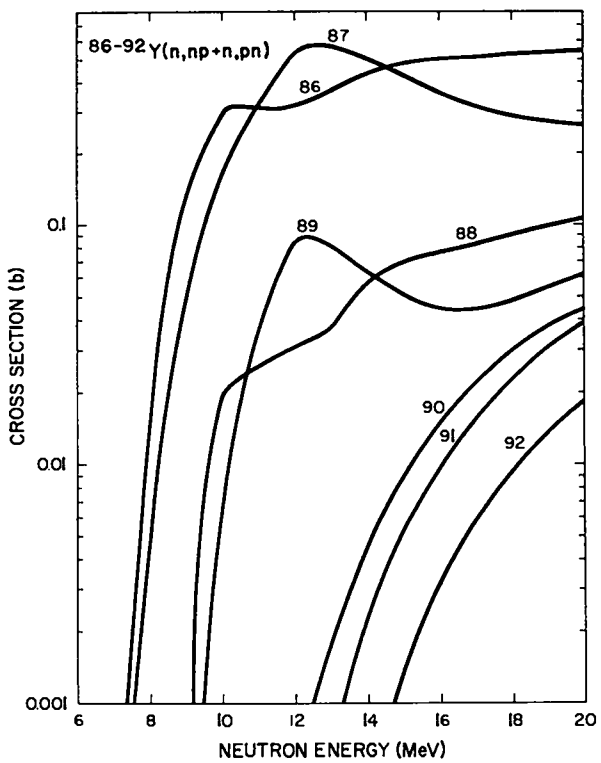

Fig. 5.
Summed $^{86-92}$Y(n,np + n,pn) cross sections. The structure in the ^{87}Y and ^{89}Y curves results from significant (n,pn) contributions before competition from the (n,2n) reaction becomes important.

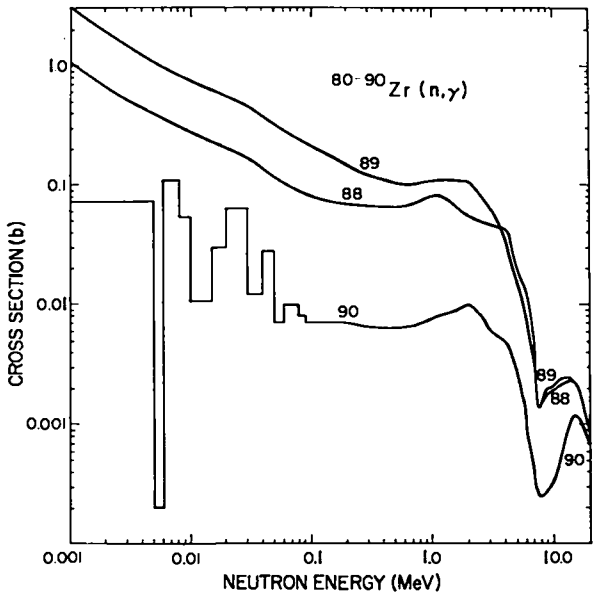

Fig. 6.
Calculated $^{88-90}Zr(n,\gamma)$ cross sections. For ^{90}Zr, the histograms result from use of average capture cross-section experimental data.

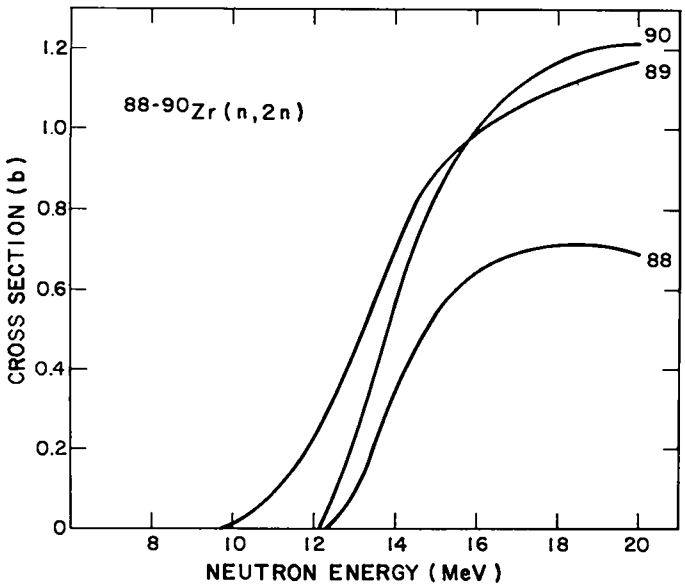

Fig. 7.
Calculated $^{88-90}Zr(n,2n)$ cross sections.

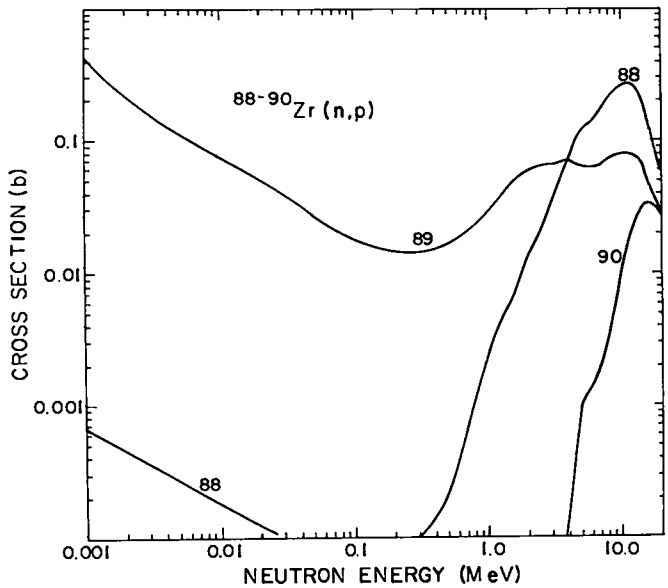

Fig. 8.
Cross sections for $^{88-90}Zr(n,p)$ reactions.

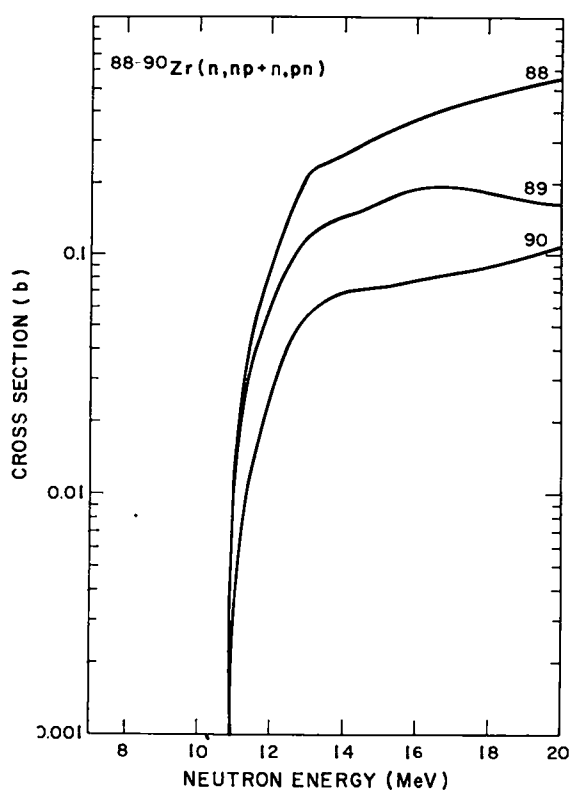

Fig. 9.
The calculated $^{88-90}Zr(n,np + n,pn)$ cross sections. The curves for $^{88,89}Zr$ lie above that for ^{90}Zr, partially because of substantial (n,pn) contributions.

In summary, these calculations employ parameters determined from a very complete analysis of both neutron and charged-particle data in this mass region. Overall, the calculations agree well with extensive comparisons to yttrium and zirconium experimental data and should, therefore, provide reasonable cross sections in regions where data are not available.

C. Fission Spectrum Workshop (L. Stewart)

A workshop was held at Brookhaven National Laboratory, Oct. 23, 1978, to discuss the status of neutron spectra from fission reactions, particularly from the viewpoint of data evaluations of fissile and fertile materials. The agenda included a general assessment of evaluator data needs [L. Stewart, Los Alamos Scientific Laboratory (LASL)], a theoretical derivation of the expected fission-spectrum shape (R. Nix, LASL), a review of the available experimental data (J. Browne, Lawrence Livermore Laboratory), a discussion of fission-spectrum effects on $\bar{\nu}$ measurements (J. R. Smith, E.G. & G. Idaho, Inc.), and a summary of fission-spectrum representations used for standards (C. Eisenhauer, National Bureau of Standards). The discussions were informal and included many contributions from the audience. Minutes will be issued that will summarize the various discussions and conclusions from the workshop.

D. Calculation of Prompt Fission Neutron Spectra [D. G. Madland and J. R. Nix (T-9)]

For the design of nuclear reactors and other applications, it is important to know the prompt fission neutron spectrum as a function of both the fissioning nucleus and its excitation energy. We study these dependences by use of standard nuclear-evaporation theory[12] to calculate the neutron energy spectrum in the fission-fragment center-of-mass system, and then transform these results to the laboratory system.

To simulate the cooling of the fragments as neutrons are emitted, we take the distribution of fission-fragment excitation energy to be rectangular in shape, extending from zero to the maximum value

$$E_m^* = E_r + B_n + E_n - E_f^{tot} \quad .$$

Here E_r is the energy release for the experimental most probable mass division, B_n and E_n are the separation energy and kinetic energy of the neutron inducing fission, and

$$E_f^{tot} = (0.1071\ Z^2/A^{1/3} + 22.2)\ \text{MeV}$$

is the total average fission-fragment kinetic energy,[13] with Z and A the atomic number and mass number of the compound nucleus undergoing fission. In calculating E_r and B_n, we use experimental masses where available and otherwise the droplet-model mass formula of Myers.[14] On the basis of the Fermi-gas model, the corresponding distribution in fission-fragment nuclear temperature is triangular in shape, extending from zero to the maximum value[15]

$$T_m = [E_m^*(8\ \text{MeV})/A]^{1/2} \quad .$$

Under the assumption that the cross section for the inverse process of compound-nucleus formation is constant, we integrate the neutron energy spectrum for fixed temperature[12] over this triangular distribution. The resulting center-of-mass spectrum, of a fission fragment moving with average kinetic energy per nucleon $E_f = E_f^{tot}/A$, is then transformed to the laboratory system. This yields for the prompt fission neutron spectrum

$$N(E) = \frac{1}{3(E_f T_m)^{1/2}} \left[u_2^{3/2} E_1(u_2) - u_1^{3/2} E_1(u_1) + \gamma(\tfrac{3}{2}, u_2) - \gamma(\tfrac{3}{2}, u_1) \right] \quad ,$$

where E is the laboratory neutron energy, $E_1(x)$ is the exponential integral,[16] $\gamma(a,x)$ is the incomplete gamma function,[16] $u_1 = (\sqrt{E} - \sqrt{E_f})^2/T_m$, and $u_2 = (\sqrt{E} + \sqrt{E_f})^2/T_m$.

For the fission of ^{235}U induced by 0.53-MeV neutrons, we compare in Fig. 10 the spectrum calculated in this way, *without the use of any adjustable parameters*, with the experimental results of Johansson and Holmquist.[17] We also show the Watt and Maxwellian distributions that are obtained by approximating the spectra in the center-of-mass and laboratory systems, respectively, by Maxwellian distributions.[18] The effective Watt temperature $T_W = \frac{8}{9} T_m$ and Maxwellian

temperature $T_M = \frac{8}{9} T_m + \frac{2}{3} E_f$ are determined by requiring that the mean energy of the original and approximate distributions be equal.

When the constants E_f and T_m are determined *a priori*, our original distribution reproduces the experimental results better than do either the Watt or Maxwellian distributions, especially at high neutron energy. The better agreement that is obtained in practice with the Watt and Maxwellian distributions is achieved by adjusting parameters[17,18] to values that are somewhat unphysical. The discrepancies that exist between the calculated and experimental spectra at neutron energies less than approximately 1 MeV could arise from our neglect of the energy dependence of the cross section for compound-nucleus formation,[12] a possibility that we are currently investigating.

Figure 11 shows how the calculated spectrum shifts to higher neutron energy, either as the fissioning nucleus increases in charge and mass from ^{236}U to ^{252}Cf, or alternatively as the incident neutron energy increases from 0.53 MeV to 14.1 MeV.* In summary, the dependence of the prompt fission-neutron spectrum upon both the fissioning nucleus and its excitation energy can be calculated straightforwardly, with constants that are determined *a priori* from other physical considerations.

E. LASL Version of NMTC (D. G. Foster, Jr.)

During the past eight years, a distinct version of the Nucleon-Meson Transport code[19] (NMTC) developed at Oak Ridge National Laboratory (ORNL) has evolved at the Los Alamos Scientific Laboratory, largely as the result of work by P. A. Seeger, with recent additions by D. G. Foster, Jr., and A. H. Wells. NMTC calculates the macroscopic transport of neutrons and charged particles by Monte Carlo methods, using Monte Carlo intranuclear-cascade and evaporation models to calculate the interactions of particles with nuclei. It is thus a very general program but quite expensive to use. In the form developed by Seeger, it uses the facilities in the Computer Development Corporation (CDC) editing utility called UPDATE to make it easy to select different versions of NMTC to suit the requirements of particular cases.

*A simple FORTRAN code FISPEK was written to perform the calculations described here. In addition, the capability exists to perform non-linear least-squares fitting analyses of measured prompt fission neutron spectra. Currently, a Marquardt non-linear least-squares routine is used to obtain fits to either the Maxwellian or the Watt distribution.

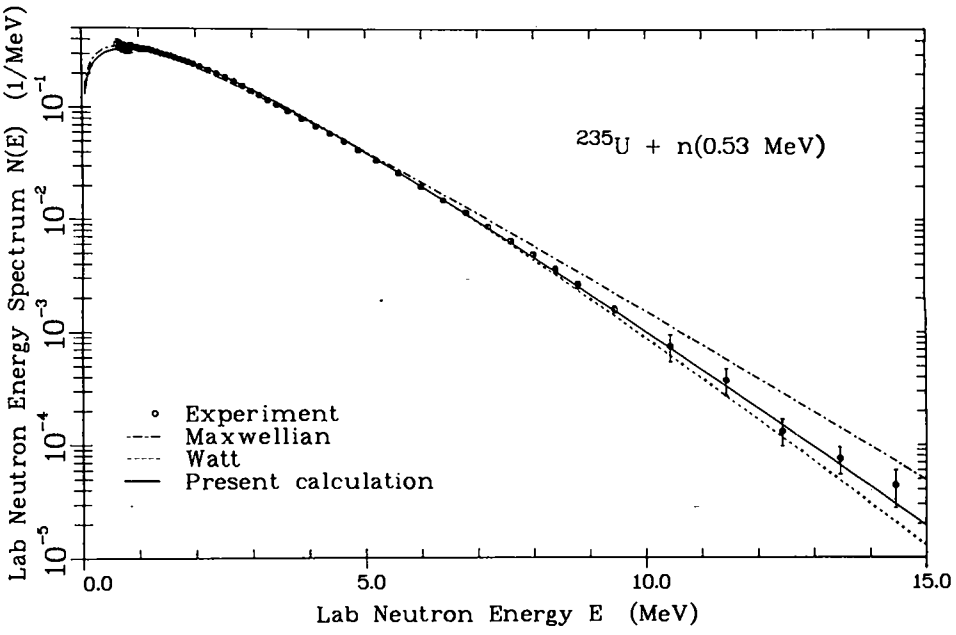

Fig. 10.

Comparison of experimental and calculated spectra. The values of the two constants in our present calculation are E_f = 0.716 MeV and T_m = 1.008 MeV whereas those in the corresponding Watt distribution E_f = 0.716 MeV and T_W = 0.896 MeV. The value of the single constant in the corresponding Maxwellian distribution is T_M = 1.373 MeV.

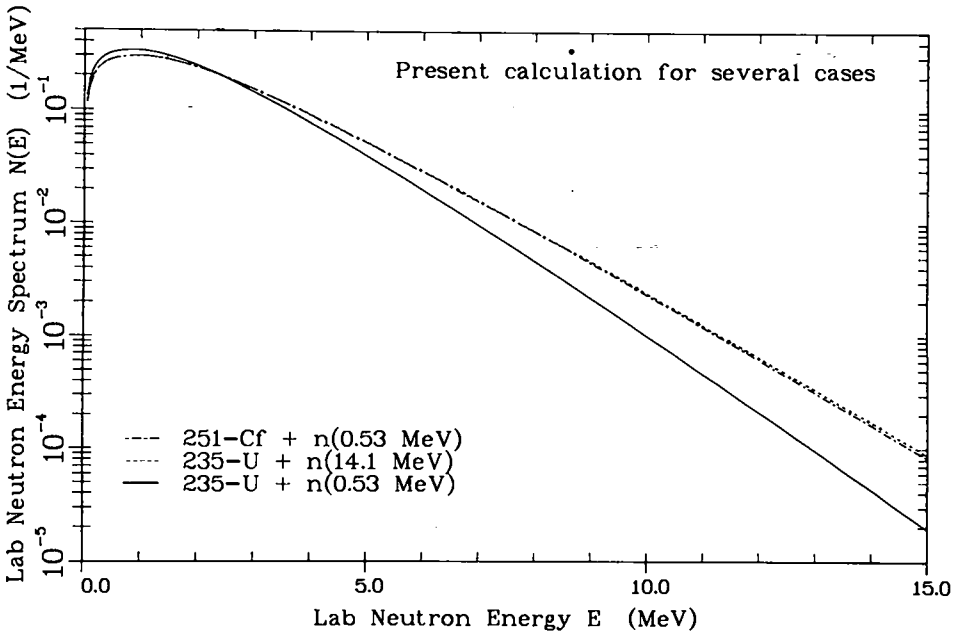

Fig. 11.

Calculated dependence of the spectrum upon the fissioning nucleus and its excitation energy. The values of the constants for ^{235}U + n (0.53 MeV) are E_f = 0.716 MeV and T_m = 1.008 MeV; for ^{235}U + n (14.1 MeV) E_f = 0.716 MeV and T_m = 1.215 MeV; and for ^{251}Cf + n (0.53 MeV) E_f = 0.734 MeV and T_m = 1.197 MeV. The spectrum for ^{235}U + n (14.1 MeV) is calculated for first-chance fission only.

This version of NMTC has now been converted into a form that can be exported to other facilites that use CDC computers with the UPDATE system. The complete program is broken down into a "fixed" and a "volatile" section, each represented by card images that will regenerate the UPDATE files used at LASL. Each of these files has a second card-image file that will induce modifications of the basic file, thus recreating the full flexibility of the LASL version as well as preserving much of the historical record of the evolution of the code. Some vestiges of the Chili Ridge Operating System (CROS) are still apparent, but they are localized and readily adapted to the specific operating systems used at other laboratories. A tape copy of the exportable form has been sent to the Sandia Laboratories in Albuquerque for an initial off-site test.

F. Summary Documentation of LASL Data Evaluations for ENDF/B-V (P. G. Young)

Summary documentation[20] has been compiled describing the nuclear data evaluations from LASL that will be included in Version V of ENDF/B. A total of 18 general purpose evaluations of neutron-induced data are summarized, together with 6 summaries directed specifically at covariance data evaluations. The general purpose evaluation summaries cover the following isotopes: $^{1-3}$H, ^{3,4}He, ^{6,7}Li, ^{10}B, ^{14,15}N, ^{16}O, ^{27}Al, $^{182-184,186}$W, ^{233}U, and ^{242}Pu. The covariance data summaries are given for ^{1}H, ^{6}Li, ^{10}B, ^{14}N, ^{16}O, and ^{27}Al. The summaries do not cover LASL work on such special purpose files as fission-product yields, activation cross sections, gas production, etc.

II. NUCLEAR CROSS-SECTION PROCESSING

A. Space-Energy Collapse (R. E. MacFarlane)

A new space-energy cross-section code is being developed to go with NJOY in the same way that SPHINX[21] goes with MINX[22] and 1DX[23] goes with ETOX.[24] This code has been named MAX for MAcroscopic X-Section Code. Like its ancestors, MAX is designed to produce self-shielded coarse-group cross sections for complex two- and three-dimensional neutron-transport problems. It will use the background cross section method with adaptations for fast reactors, thermal reactors, and shielding. It will explicitly treat prompt and delayed photon production and transport, prompt and delayed heating, and depletion.

This new system began to take shape this quarter when the TRANSX code and MATXS interface file described in previous reports were linked to the LASL one-dimensional discrete-ordinates transport code ONETRAN-DA. In collaboration with

Gene Bosler of the Transport Theory Group (T-1), an efficient link was designed and installed in ONETRAN-DA. The resulting system has all the capabilities of 1DX and all those of SPHINX except for the automatic calculation of Dancoff factors. The system adds the following capabilites: elastic matrix self-shielding, shielded heating and photon production, coupled neutron-photon transport, shielding and collapse of P_ℓ matrices, thermal upscatter, intermediate resonance shielding, composition-dependent fission spectra, and flexible response function activity edits.

The prototype system has been tested on the fast spectrum benchmarks[25] JEZEBEL AND GODIVA with results very similar to those obtained with MINX/ONETRAN. Tests on the thermal benchmarks[25] TRX-1, ORNL-2, and BAPL-1 were executed successfully, but they revealed some problems: outer iteration convergence is slow for upscatter using ONETRAN-DA, there is a slight imbalance in the thermal data, and the resonance integrals are somewhat higher than those obtained by other methods. The first problem will be attacked by adding outer-iteration acceleration to the transport module, the second should be improved by the new angular quadrature discussed in Sec. II.B., and the third is now under investigation.

B. Discrete Angle Representation of Thermal Neutron Scattering [R. E. MacFarlane and R. Prael (TD-6)]

The angle dependence of thermal neutron scattering is complex. Cross section vs scattering cosine can be isotropic, strongly backward-peaked, strongly forward-peaked, or even-peaked around some intermediate angle. Because of this variation, a truncated Legendre expansion may sometimes be a poor representation of the differential cross section. This problem shows up clearly when converting Legendre cross sections back to the angular domain for use in Monte Carlo codes -- the resulting scattering function will often have nonphysical negative values. The same variation makes it difficult to perform the angular integrations required to obtain the Legendre cross sections required by multigroup transport codes. In order to solve both these problems, and in order to provide as much consistency as possible between Monte Carlo and multigroup data sets, a new representation of the pointwise thermal cross sections produced by the THERMR module of NJOY has been developed.

This representation is based on discrete angles. For incoherent inelastic scattering, the differential cross section for a given initial energy E is determined adaptively so that the cross section for any secondary energy E' can be

computed to within a specified tolerance using linear interpolation. At the same time, the angular dependence for each E and E' is also determined adaptively. This angular dependence is then resolved into a set of equally probable cosine ranges, and the single discrete cosine that preserves the average value cosine for each bin is chosen. Additional E' grid points are added if necessary so that the equally probable cosines can be determined as functions of E' by linear interpolation. These results are saved for subsequent use on a pointwise-ENDF (PENDF) file.

For use in a Monte Carlo code, the secondary energy dependence can be converted to equally probable energies by a subsequent code. The result is a set of equally probable energy-angle phase-space events ideally suited for random sampling. The relatively large number of collisions expected in the thermal range will average out the discrete nature of the representation for most problems.

For use in multigroup transport codes, the angular delta functions are easily integrated to obtain Legendre coefficients. Strongly peaked functions retain enough characteristic information to make high Legendre order possible. Although the P_2 and higher components are only correct in the limit of many bins, the truncation should be no more serious than the natural truncation inherent in S_N transport codes. This representation is readily interpolable in E when performing the integrations over incident energy required for the group-to-group cross sections. The spectrum at each E grid point is divided into equally probable bins. For E in (E_i, E_i+1), the j^{th} bin at E_i is connected to the j^{th} bin at E_{i+1} using linear interpolation for E' and each of the equally probable scattering angles. In this way, a smooth representation of the Legendre components of group-to-group scattering is obtained with a relatively coarse incident energy grid.

Incoherent elastic scattering as found in the ENDF/B representations[26] of the scattering from zirconium hydride and polyethylene can be represented by a cross section and a set of equally probable angles vs incident energy. The angles can be computed analytically from the cross section

$$\sigma^{iel}(E,\mu) = \frac{\sigma_b}{2} e^{-\frac{2EW}{A}(1-\mu)},$$

where σ_b is the bound cross section, W is a Debye-Waller factor, A is the scatterer mass ratio, and μ is the scattering cosine.

Coherent elastic scattering from randomly oriented hexagonal crystallites (e.g., graphite) cannot be represented by equally probable angles. Here the scattering is naturally discrete. The cross section can be expressed in the form

$$\sigma^{coh}(E,\mu) = \sum_{i=1}^{I} \frac{b_i}{E} \delta(\mu-\mu_i) \quad ,$$

where

$$\mu_i = 1 - 2\frac{E_i}{E} \quad ,$$

where the E_i are the energies of the Bragg "edges," and where the sum extends over all i such that $E_i < E$. Note that the E_i and b_i can easily be determined from the cross section computed in the traditional way by HEXSCAT[27] or NJOY. *The entire angular distribution is implicit in the P_0 cross section.* The representation using E_i and b_i compactly describes the strong backward peaks seen near each Bragg edge.

These discrete angle methods have been coded into NJOY and are now being tested using the LASL Monte Carlo code MCNP and several multigroup thermal reactor codes.

C. Testing Data and Methods Effects on JEZEBEL and GODIVA (R. B. Kidman)

Some recent LASL calculations of the Cross Section Evaluation Working Group (CSEWG) fast reactor benchmarks[28] JEZEBEL and GODIVA yielded eigenvalues of 1.00850 and 0.99399, respectively. The central fission rate ratios of ^{238}U and ^{235}U were also computed, and the quotients of the calculated values to the experimental values were found to be 0.93009 and 1.05649, respectively. Those calculations are characterized by the following data and options:

(a) 50-group library,

(b) based on preliminary ENDF/B-V,[29]

(c) self-shielded,

(d) 10 inelastic downscatter terms,

(e) elastic removal iteration,

(f) S_{16} angular quadrature,

(g) transport approximation, and

(h) utilized old fission sources.[30]

The central fission rate ratios are disturbing because the ^{238}U and ^{235}U cross sections are supposedly known to a greater precision than indicated by the ratios. Since LASL is responsible for JEZEBEL and GODIVA, a study was initiated to determine if a better choice of data or options would remove the difficulty.

The options studied included various group structures, fission sources, and cross-section sources. Also investigated were the effects of self-shielding, elastic removal iteration, full elastic and inelastic matrices, angular quadratures, and Legendre order. The results are presented in Table II. In the table, PRE-V refers to preliminary ENDF/B-V, and LIB-IV refers to ENDF/B-IV.

It is obvious from the table that no single option or reasonable combination of options will yield central fission rate ratios that adequately agree with experiment.

In the course of carrying out these calculations, it became evident that the benchmark writeups for JEZEBEL and GODIVA are deficient in several respects. First, the correction given for gallium in JEZEBEL is based on old cross-section data. This should be updated and also, for the sake of completeness, the actual gallium density should be specified in the benchmark.

Second, the value of β_{eff} used in converting the experimental material worths at core center for both JEZEBEL and GODIVA is obsolete; the original experimental numbers should be included in the benchmark writeups.

Finally, the leakage spectra given in the two benchmarks are normalizations and coarse groupings of the original data. Again, the original data, with errors, should be included in each benchmark.

LASL will undertake the task of rewriting these two benchmarks and submitting the rewrites to the CSEWG Data Testing Subcommittee for consideration as replacements to the present writeups.

D. Gamma-Ray Spectra of Activation Products (M. E. Battat and R. J. LaBauve)

Two libraries of gamma lines for selected radionuclides have been obtained and made available at LASL. The first library,[31,32] compiled at Kernforschungsanlage (KFA), Julich, Germany, was obtained from the Nuclear Data Section of the International Atomic Energy Agency (IAEA) in Vienna, Austria, and contains data for about 1200 nuclides. As received, the number of gamma-ray lines for each

TABLE II

SPECIFIC EFFECTS

Testing (with respect to)	Effect on Multiplication Factor		Effect on Central Fission Ratio $\left(\frac{\text{U-238}}{\text{U-235}}\right)_C \Big/ \left(\frac{\text{U-238}}{\text{U-235}}\right)_E$	
	JEZEBEL	GODIVA	JEZEBEL	GODIVA
PRE-V (LIB-IV)	0.00870	-0.01726	0.00801	0.00367
PRE-V Composition Chi (Old Chi)	-0.00019	-0.00162	0.01420	0.01141
LIB-IV Composition Chi (Old Chi)	-0.00042	-0.00066	0.00366	-0.00982
PRE-V X-sec and Chi (LIB-IV X-sec and Chi)	0.00893	-0.01822	0.02587	0.02490
185-Group (50-Group)	-0.00008	-0.00104	-0.00087	-0.00169
240-Group (50-Group)	-0.00035	-0.00109	-0.00410	-0.00934
Full Inelastic Scattering Matrix (10 Downscattering Terms)	0.00002		0.00076	
Full Elastic Scattering Matrix (One Elastic Removal Term)	0.		-0.00001	
Elastic Removal Iteration (No Iteration)	0.	-0.00012	0.00009	0.00002
Self-Shielding (Infinite Dilution)	0.00010	0.00013	-0.00017	-0.00031
P_3 (Transport Approximation)	-0.00337	-0.00344	0.00030	-0.00019
P_3 (P_0)	-0.08887	-0.10940	-0.00750	-0.01195
P_3 (P_1)	0.00596	0.00527	0.00845	0.00977
P_3 (P_2)	-0.00010	-0.00004	-0.00145	-0.00109
S_{48} (S_2)	-0.04697	-0.03550	0.01122	0.01169
S_{48} (S_4)	-0.01318	-0.00909	0.00120	-0.00119
S_{48} (S_8)	-0.00356	-0.00243	0.00038	-0.00010
S_{48} (S_{16})	-0.00088	-0.00060	0.00014	0.00007
S_{48} (S_{32})	-0.00014	-0.00010	0.00002	0.00003
S_∞ (S_{48})	-0.00009	-0.00009		

nuclide was specified in a free-field format. A code was written to convert the free-field format to one with a fixed field. The second library[33] was received from the Radiation Shielding Information Center (RSIC) at the Oak Ridge National Laboratory (ORNL). This library gives data on the atomic and nuclear radiations emitted by 240 radionuclides. The Julich library, and possibly the ORNL library, will be used to generate a multigroup library of gamma-ray yields for use with the MONTAGE-400 data package,[34] which contains 100-group neutron activation cross-section data for fusion reactor structure and coolant materials.

III. FISSION PRODUCTS AND ACTINIDES: YIELDS, YIELD THEORY, DECAY DATA, DEPLETION, AND BUILDUP

A. Fission Yield Theory [R. E. Pepping and C. W. Maynard (University of Wisconsin); D. G. Madland; T. R. England; and P. G. Young]

In order to improve the yield calculation, a more realistic formulation of the evaluation of the density of nuclear states is under investigation. A copy of the Moretto density code[35] has been obtained. A guide for the use of this code has been written and is available. We would like to express our thanks to Professor L. G. Moretto and Mr. Lee Sabotka of the University of California, Berkeley, for their assistance in obtaining and understanding this code. A revised version is also available, which requires about half of the computation time of the original version. Work is currently underway to produce a much faster version that will allow the user to assemble the required thermodynamic functions for the evaluation of the densifiers from sets of spline coefficients approximating these functions for the number of neutrons and protons desired. Initial investigations indicate such spline approximations to be accurate to a few per cent.

In order to simplify the evaluation of the convolution integral required to compute the fission-fragment yields, the saddle-point approximation has been examined. The state density is assumed to be given by

$$\rho(E) \propto \exp\ (2\ \sqrt{aE}) \quad .$$

Numerical evaluation of the convolution integral,

$$\int_0^E \rho_1(E_1)\ \rho_2\ (E-E_1)\ dE_1 \quad ,$$

was performed with 50- and 100-point Simpson rules, the two methods giving results which differ by less than 2 parts in 10^4. The saddle-point approximation yielded results differing by less than 10% from the 100-point Simpson rule cases examined. The error in using the saddle-point approximation for the evaluation of the yield integral,

$$\int_0^E \rho(k) \int_0^{E-k} \rho_1(E_1)\ \rho_2\ (E-k-E_1) dE_1\, dk \quad ,$$

where k is the translational kinetic energy and $\rho(k)$ is the density of translational states, remains to be evaluated.

B. ENDF/B-V Yields (T. R. England, J. Liaw (University of Oklahoma) and N. L. Whittemore)

Cumulative mass-chain yields and uncertainties were listed in the last progress report. A draft of the extensive data tests has been completed but will be expanded into a more general report for use as a reference on ENDF/B-V yields. Currently, the completed yield compilation is being compared for consistency in isomeric state identifications with the incomplete decay-data files, and an ENDF/B-IV yield library is being generated for the CINDER-10 code.

C. ENDF/B-V Average Energies (T. R. England and N. L. Whittemore)

The ENDF/B-V decay format (MT 457) is greatly expanded from that of Version IV. It permits more detail for decay types and a larger variety of decay spectra than ENDF/B-IV. Currently, only a preliminary set of spectral data exists in the new format (269 nuclides). For these, only 47 have computed average energies.

We prepared a code to process the spectra; to compute average energies, Q values, etc.; and to compare results with Version IV data. There are large differences in many cases (e.g., ∿120 exceed 5% even in total energy, and most of these exceed 10%). The differences were reported to the Chairman of the CSEWG Fission Product and Actinide Subcommittee.

The code will be expanded to include additional tests appropriate for Phase I review of ENDF/B-V decay data and ultimately to provide multigroup spectra and partial input libraries for CINDER-10.

D. CINDER-10/ORIGEN Comparison (T. R. England and N. L. Whittemore)

Allen Croff from ORNL requested a comparison between ORIGEN and CINDER-10 following a 10^{13} s thermal irradiation of ^{235}U (no depletion and no absorption permitted). CINDER-10 uses ENDF/B-IV data. ORIGEN has been distributed with various libraries (dependent on the distribution date). The most recent ORIGEN library uses a mixture of ENDF/B-IV and ENSDF data. Results on total aggregate heating for the particular case compared are in better agreement than values reported using other ORIGEN libraries and more realistic power histories.

A comparison of all nuclides contributing ∿1% of the total heating was supplied to ORNL. Differences of 5-10% were typical, but several large differences (10 to 100%) exist. However, the aggregate heating agreed within 1-4%, depending on the cooling time.

Many of the individual nuclide differences were examined in detail, and most of the differences on the order of 10% could be attributed to the use of ENSDF data in ORIGEN. For these, we also compared several decay energies from the preliminary ENDF/B-V data and found even larger differences. Some of the larger differences examined could not be attributed to nuclide parameters. This effort was discontinued until ENDF/B-V data becomes available and the new ORIGEN library is expanded to include beta and gamma energies rather than total (recoverable) energy.

E. Fission Product Gamma Spectra [E. T. Jurney (P-DO), P. J. Bendt (P-2), and T. R. England]

The fission product gamma spectra of ^{233}U, ^{235}U, and ^{239}Pu have been measured at 12 cooling times following 20 000 s irradiations in the thermal column of the Omega West Reactor. The mean cooling times ranged from 29 to 146 500 s. The total gamma energies were obtained by integrating over the energy spectra, and both the spectra and the total energies are compared with calculations using the CINDER-10 code and ENDF/B-IV data.

The measured and calculated gamma spectra are compared in a series of figures. The measured total gamma energies are ∿14% larger than the calculated energies during the earliest counting period (4-54 s cooling time). For ^{235}U, the measured and calculated total gamma energies are nearly the same after 1200 s cooling time, and the measurements are 2-6% lower at longer cooling times. For ^{239}Pu, the measured and calculated total gamma energies are nearly the same at cooling times longer than 4000 s, and for ^{233}U, this condition prevails at cooling times longer than 10 000 s.

The calculations are for the release rate at the midpoint of the counting interval. Except for the first interval of 4-54 s, this agrees with an average over the counting interval within ∿1%. During the first interval, the decay energy changes by nearly a factor of two, and an average is necessary. This reduces the largest disagreement to ∿9.5%.

This work is now completed and reported in Ref. 36. In addition, an invited paper comparing calculations with recent measurements of beta and gamma spectra at the University of Illinois and ORNL was prepared for Nuclear Technology in October 1978.

F. The Effects of Neutron Absorption on Decay Heat (R. J. LaBauve, T. R. England, and W. B. Wilson)

Neutron absorption by fission products becomes important at high-flux levels and long cooling times. There are two effects of absorption; namely, the flux level can reduce the density of directly yielded products in the fission pulse, significant for nuclides having large cross sections and large yields, and nuclide-coupling in stable and long-lived nuclides tends to buildup the concentration of more unstable nuclides. General equations are developed in Appendix D of Ref. 37 for approximating both positive and negative effects of absorption with two-nuclide chains. Also, the equations in Ref. 37 are given for two incident neutron-energy groups (thermal and epithermal).

If simplifications are made to the equations in Ref. 37 so that only positive effects of the neutron absorption are taken into consideration and only cases with constant fluxes for constant irradiation times are treated, then the absorption correction for a reaction such as $^{133}Cs(n,\gamma)^{134}Cs$, discussed in Ref. 37, is given by the equation

$$F(t,T,\phi) = N(T,\phi)\lambda_2 E_G e^{-\lambda_2 t} \quad , \tag{1}$$

where the correction F is the decay energy to be added to the calculation without absorption, t is the cooling time, λ_2 is the decay constant of the second nuclide in the two-nuclide chain (^{134}Cs in the above example), E_G is the average gamma- or beta-energy for energy group G for nuclide 2, and $N(T,\phi)$ is the additional atom density of nuclide 2 resulting from radiative capture in nuclide 1:

$$N(T,\phi) = Y_1 A_1 K \left[\frac{1}{\beta_1\beta_2} - \frac{e^{-\beta_1 T}}{\beta_1(\beta_2-\beta_1)} + \frac{e^{-\beta_2 T}}{\beta_2(\beta_2-\beta_1)} \right] . \tag{2}$$

Radiative capture in nuclide 2 must also generally be included, as it is in Ref. 37, but can be ignored in this approximation.

In the equation for $N(T,\phi)$, Y_1 is the fission yield for the precursor nuclide in the chain (^{133}Cs in the example), T is the irradiation time at constant power represented by a thermal flux ϕ_{th} and an epithermal flux ϕ_{epi}, and K is a units constant. Let the thermal and epithermal cross sections in the two nuclides involved in the (n,γ) reaction be represented by σ^1_{th} and σ^1_{epi} for the first nuclide and σ^2_{th} and σ^2_{epi} for the second nuclide. Also let

$$R = \phi_{epi}/\phi_{th} \quad . \tag{3}$$

Then,

$$A_1 = (\sigma^1_{th} + R\,{}^1_{epi}) \times 10^{-24}\phi_{th} \quad , \tag{4}$$

$$A_2 = (\sigma^2_{th} + R\,{}^2_{epi}) \times 10^{-24}\,\phi_{th} \quad , \tag{5}$$

$$\beta_1 = A_1 + \lambda_1 \quad , \tag{6}$$

$$\beta_2 = A_2 + \lambda_2 \quad . \tag{7}$$

Note that the yield of nuclide 1 in the chain may be affected by exposure of its precursors to high fluence. This effect is important for the two-nuclide chain $^{155}Eu(n,\gamma)^{156}Eu$. The chain structure[38] used in the EPRI-CINDER code for producing ^{156}Eu is shown in Fig. 12. This multicapture effect of fluence on precursors was examined by running a series of EPRI-CINDER problems in which fluence was varied, and the contributions to the total production of ^{156}Eu from the various chains shown in Fig. 12 were edited. Let

$$Y_1^{eff} = Y_1^C + Y_1^F \quad , \tag{8}$$

where Y_1^{eff} is the effective yield for nuclide 1, (^{155}Eu), Y_1^C the cumulative yield of nuclide 1 from fission, and Y_1^F a contribution to the effective yield of nuclide 1 from absorption reactions of the precursors of nuclide 1. Proportioning number densities to yields,

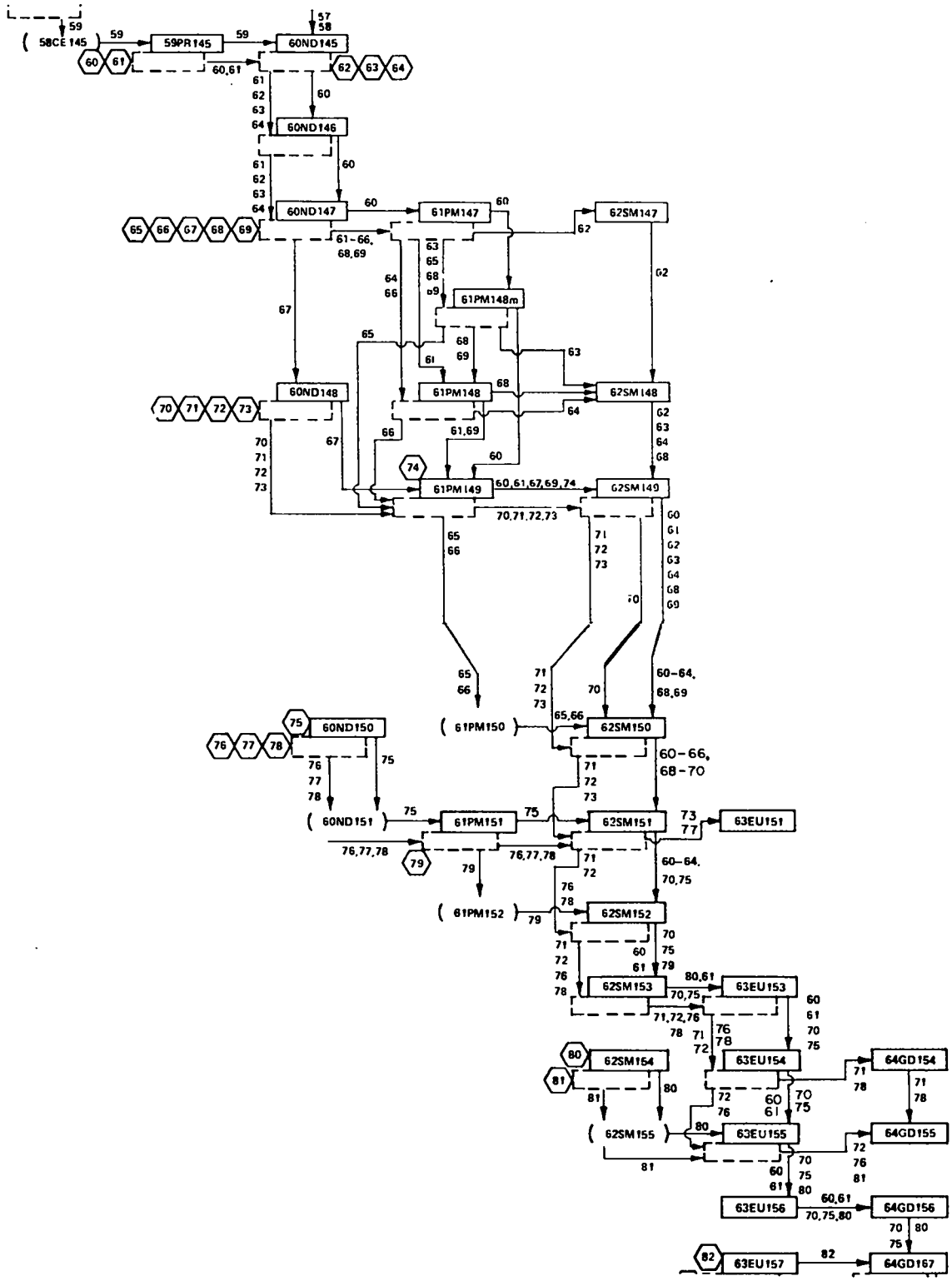

Fig. 12.
EPRI-CINDER chains leading to ^{155}Eu.

$$\frac{Y_1^C}{P_c} = \frac{Y_1^{eff}}{P_T} , \tag{9}$$

or

$$Y_1^F = \frac{P_T - P_c}{P_c} \; Y_1^C , \tag{10}$$

where P_T is the total number density of nuclide 2 (^{156}Eu), and P_C is the production number density of nuclide 2 from a special chain edited in the EPRI-CINDER runs consisting only of the two nuclides [$^{155}Eu(n,\gamma)^{156}Eu$].

The result of this EPRI-CINDER study is shown graphically in Fig. 13, where the quantity Y_1^F is plotted against fluence. Note that double points are shown in the figure for problems in which different combinations of fluxes and irradiation times were used to give the same fluence. Also note the two-segment fits indicated in the figure that are used to approximate this effect.

The equations above, including the fits for the multiple absorption effect, were coded for a pocket calculator (TI-59), and the problems were run, which included only three two-nuclide chains, namely, $^{133}Cs(n,\gamma)^{134}Cs$, $^{147}Pm(n,\gamma)^{148}Pm$, and $^{155}Eu(n,\gamma)^{156}Eu$. Since the half-lives of ^{134}Cs, ^{148m}Pm, and ^{156}Eu are 6.5×10^7 s, 3.6×10^6 s, and 1.3×10^6 s, respectively, the absorption corrections for these three two-nuclide chains are most important for the cooling time range from about 5×10^5 s to 1×10^8 s.

Table III gives comparisons of the TI-59 approximate calculations with the more accurate summation results of the CINDER-10 code.[39] As can be seen from the table, the three chains used in the approximate TI-59 calculation account for most of the absorption effects in this time range.

REFERENCES

1. H. M. Agnew, W. T. Leland, H. V. Argo, R. W. Crews, A. H. Hemmendinger, W. E. Scott, and R. F. Taschek, "Measurement of the Cross Sections for the Reaction T + T → ^{4}He + 2n + 11.4 MeV," Phys. Rev. 84, 862 (1951)

2. G. M. Hale and P. G. Young, "T(t,2n)^{4}He Reaction," in "Applied Nuclear Data Research and Development July 1-September 30, 1978," Los Alamos Scientific Laboratory report LA-7596-PR (December 1978).

3. D. M. Holm and H. V. Argo, "t-t Elastic Scattering from 1.6 to 2.0 MeV," Phys. Rev. 101, 1772 (1956).

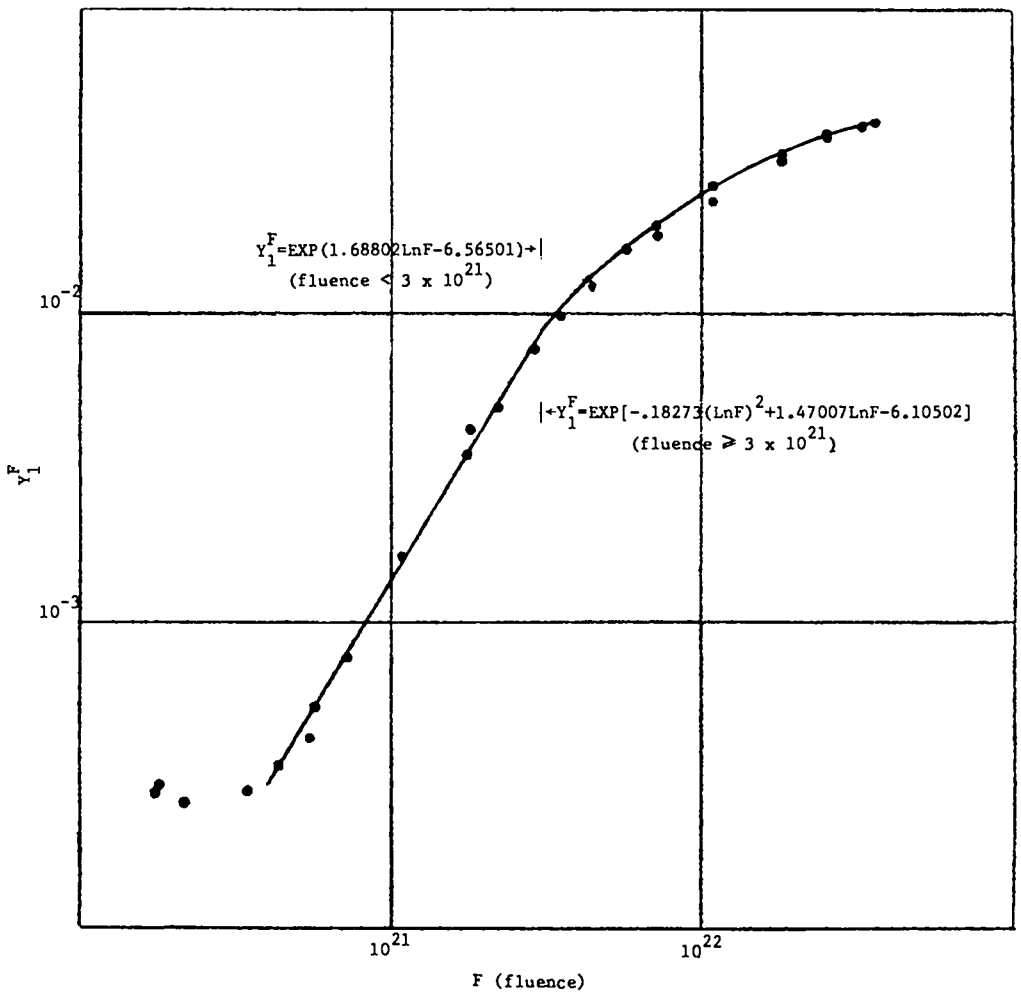

Fig. 13.
Precursor contributions to the effective yield of ^{155}Eu as a function of fluence.

4. Ch. Lagrange, "Optical Model Parameterization between 10 keV and 20 MeV - Application to the ^{89}Y and ^{93}Nb Spherical Nuclei," presented at the National Soviet Conference on Neutron Physics (1975).

5. C. H. Johnson, A. Galonsky, and R. Kernell, "Anomalous Optical Model Potential for Sub-Coulomb Protons for $89 \leqslant A \leqslant 130$," Phys. Rev. Lett. 39, 1604 (1977).

6. E. D. Arthur, "Calculation of the ^{88}Y(n,γ) Cross Section Using Gamma-Ray Strength Functions," in "Applied Nuclear Data Research and Development January 1-March 31, 1978," Los Alamos Scientific Laboratory report LA-7301-PR (June 1978).

7. E. D. Arthur and P. G. Young, "Neutron Cross Sections for Yttrium and Titanium Isotopes," in "Applied Nuclear Data Research and Development April 1-June 30, 1977," Los Alamos Scientific Laboratory report LA-6971-PR (Sept. (September 1977).

TABLE III

NEUTRON ABSORPTION EFFECTS -- COMPARISON OF APPROXIMATE METHOD WITH CINDER-10

Cooling Time (s)	Group 1 0.1-0.4 MeV		Group 2 0.4-0.9 MeV		Group 3 0.9-1.35 MeV		Group 4 1.35-2.2 MeV		Group 5 2.2-2.6 MeV		Group 6 2.6-3 MeV	
	TI-59	CINDER	TI-59	CINDER	TI-59	CINDER	TI-59	CINDER	TI-59	CINDER	TI-59	CINDER
$1. \times 10^{5}$	2.0	-3.3	214.5	265.8	102.3	125.0	9.8	95.0	70.9	72.1	4.0	8.5
$5. \times 10^{5}$	1.7	3.4	206.5	215.7	83.8	94.2	8.9	24.9	57.3	57.5	3.2	3.7
$1. \times 10^{6}$	1.4	1.1	198.1	199.6	65.5	71.4	8.0	10.9	44.1	43.9	2.5	2.4
$5. \times 10^{6}$	0.2	-0.5	167.8	163.7	11.7	11.8	5.3	4.9	5.3	5.2	0.3	0.3
$1. \times 10^{7}$	0.0	-0.1	154.8	151.0	4.2	4.1	4.6	4.5	0.4	0.3	0.0	0.0
$5. \times 10^{7}$	0.0	-0.2	100.1	98.9	2.2	2.1	3.0	2.9	0.0	-0.2	0.0	0.0
$1. \times 10^{8}$	0.0	0.0	58.7	58.7	1.3	1.3	1.8	1.7	0.0	0.0	0.0	0.0
$5. \times 10^{8}$	0.0	0.0	0.8	1.7	0.0	0.0	0.0	0.0	0.0	0.0	0.0	0.0
$1. \times 10^{9}$	0.0	0.0	0.0	0.2	0.0	0.0	0.0	0.0	0.0	0.0	0.0	0.0

FLUX = 1×10^{14} n/cm^2-s

IRRADIATION TIME = 7.2×10^{7} s

TARGET = ^{235}U

INCIDENT NEUTRON ENERGY = Thermal

Table given for photon decay energy in MeV/s.

8. A. Gilbert and A. G. W. Cameron, "A Composite Nuclear Level Density Formula with Shell Corrections," Can. J. Phys. 43, 1446 (1965).

9. J. L. Cook, H. Ferguson, and A. R. de L. Musgrove, "Nuclear Level Densities in Intermediate and Heavy Nuclei," Aust. J. Phys. 20, 477 (1967).

10. C. Kalbach, "The Griffin Model, Complex Particles, and Direct Nuclear Reactions," Z. Phys. A283, 401 (1977).

11. E. D. Arthur, "Calculation of Proton Production From n + ^{88,89}Y Reactions," in "Applied Nuclear Data Research and Development April 1-June 30, 1978," Los Alamos Scientific Laboratory report LA-7482-PR (September 1978).

12. V. Weisskopf, "Statistics and Nuclear Reactions," Phys. Rev. 52, 295 (1937).

13. V. E. Viola, Jr., "Correlation of Fission Fragment Kinetic Energy Data," Nucl. Data A, 1, 391 (1966).

14. W. D. Meyers, Droplet Model of Atomic Nuclei (IFI/Plenum Data Co., New York, 1977).

15. J. R. Huizenga and L. G. Moretto, "Nuclear Level Densities," Ann. Rev. Nucl. Sci. 22, 427 (1972).

16. M. Abramowitz and I. A. Stegun, Eds., Handbook of Mathematical Functions, (National Bureau of Standards, Washington D.C., 1964), pp. 227-266.

17. P. I. Johansson and B. Holmquist, "An Experimental Study of the Prompt Fission Neutron Spectrum Induced by 0.5-MeV Neutrons Incident on Uranium-235," Nucl. Sci. Eng. 62, 695 (1977).

18. J. Terrell, "Fission Neutron Spectra and Nuclear Temperatures," Phys. Rev. 113, 527 (1959).

19. W. A. Coleman and T. W. Armstrong, "The Nucleon-Meson Transport Code NMTC," Oak Ridge National Laboratory report ORNL-4606 (October 1970).

20. P. G. Young, "Summary Documentation of LASL Nuclear Data Evaluations for ENDF/B-V," Los Alamos Scientific Laboratory report LA-7663-MS (January 1979).

21. W. J. Davis, M. B. Yarbrough, and A. B. Bortz, "SPHINX: A One Dimensional Diffusion and Transport Nuclear Cross Section Processing Code," Westinghouse Electric Corporation report WARD-XS-3045-17 (August 1977).

22. C. R. Weisbin, P. D. Soran, R. E. MacFarlane, D. R. Harris, R. J. LaBauve, J. S. Hendricks, J. E. White, and R. B. Kidman, "MINX, A Multigroup Interpretation of Nuclear X-Sections from ENDF/B," Los Alamos Scientific Laboratory report LA-6486-MS (1976).

23. R. W. Hardie and W. W. Little, "1DX, A One-Dimensional Diffusion Code for Generating Effective Nuclear Cross Sections," Battelle Northwest Laboratory report BNWL-954 (1969).

24. R. E. Schenter, J. L. Baker, and R. B. Kidman, "ETOX, A Code to Calculate Group Constants for Nuclear Reactor Calculations," Battelle Northwest Laboratory report BNWL-1002 (1969).

25. E. M. Bohn, R. Maerker, B. A. Magurno, F. J. McCrossen, and R. E. Schenter, Eds., "Benchmark Testing of ENDF/B-IV," Brookhaven National Laboratory report BNL-NCS-21118 (ENDF-230) Vol. I (1976).

26. J. V. Koppel and D. H. Houston, "Reference Manual for ENDF Thermal Neutron Scattering Data," General Atomic report GA-8774 (revised July 1978 and available as ENDF-269 from the National Nuclear Data Center at Brookhaven National Laboratory).

27. Y. D. Naliboff and J. V. Koppel, "HEXSCAT, Coherent Elastic Scattering of Neutrons by Hexagonal Lattices," General Atomic report GA-6026 (1964).

28. H. Alter, R. B. Kidman, R. LaBauve, R. Protsik, and B. A. Zolatar, "ENDF-202 Cross Section Evaluation Working Group Benchmark Specifications," Brookhaven National Laboratory report BNL-19302 (1974).

29. D. Garber, Ed., "Data Formats and Procedures for the ENDF Neutron Cross Section Library," Brookhaven National Laboratory report BNL-50274 (1976).

30. R. B. Kidman, "ENDF/B-IV, LIB-IV, and the CSEWG Benchmarks," Los Alamos Scientific Laboratory report LA-7355-MS (June 1978).

31. G. Erdtmann and W. Soyka, "The Gamma-Ray Lines of Radionuclides, Ordered by Atomic and Mass Number. Part I. Z = 2-57 (Helium-Lanthanum)," J. Radioanal. Chem. 26, 375-495 (1975).

32. G. Erdtmann and W. Soyka, "The Gamma-Ray Lines of Radionuclides, Ordered by Atomic and Mass Number. Part II. Z = 58-100 (Ce-Fm)," J. Radioanal. Chem. 27, 137-286 (1975).

33. D. C. Kocher, "Nuclear Data for Radionuclides Occurring in Routine Releases from Nuclear Fuel Cycle Facilities," Oak Ridge National Laboratory report ORNL/NUREG/TM-102 (1977).

34. Radiation Shielding Information Center DLC-33/MONTAGE data package (1978).

35. L. G. Moretto, "Statistical Description of Deformation in Excited Nuclei and Disappearance of Shell Effects with Excitation Energy," Nucl. Phys. A182 641 (1972).

36. E. T. Jurney, P. J. Bendt, and T. R. England, "Fission Product Gamma Spectra," Los Alamos Scientific Laboratory report LA-7620-MS (December 1978).

37. R. J. LaBauve, T. R. England, D. C. George, and M. G. Stamatelatos, "The Application of a Library of Processed ENDF/B-IV Fission-Product Aggregate Decay Data in the Calculation of Decay-Energy Spectra," Los Alamos Scientific Laboratory report LA-7483-MS (September 1978).

38. T. R. England, W. B. Wilson, and M. G. Stamatelatos, "Fission Product Data for Thermal Reactors Part 1: A Data Set for EPRI-CINDER Using ENDF/B-IV," Los Alamos Scientific Laboratory report LA-6745-MS (EPRI NP-356) (Dec. 1976).

39. T. R. England, R. Wilczynski, and N. L. Whittemore, "CINDER-7: An Interim Report for Users," Los Alamos Scientific Laboratory report LA-5885-MS (February 1975).

☆U.S. Government Printing Office: 1979 – 677-013/50